Soft Matter

PAPER

View Article Online
View Journal

Cite this: DOI: 10.1039/c5sm01005e

Direct *in situ* measurement of specific capacitance, monolayer tension, and bilayer tension in a droplet interface bilayer†

Graham J. Taylor,[a] Guru A. Venkatesan,[a] C. Patrick Collier[b] and Stephen A. Sarles*[a]

Received 27th April 2015,
Accepted 5th August 2015

DOI: 10.1039/c5sm01005e

www.rsc.org/softmatter

Thickness and tension are important physical parameters of model cell membranes. However, traditional methods to measure these quantities require multiple experiments using separate equipment. This work introduces a new multi-step procedure for directly accessing *in situ* multiple physical properties of droplet interface bilayers (DIB), including specific capacitance (related to thickness), lipid monolayer tension in the Plateau–Gibbs border, and bilayer tension. The procedure employs a combination of mechanical manipulation of bilayer area followed by electrowetting of the capacitive interface to examine the sensitivities of bilayer capacitance to area and contact angle to voltage, respectively. These data allow for determining the specific capacitance of the membrane and surface tension of the lipid monolayer, which are then used to compute bilayer thickness and tension, respectively. The use of DIBs affords accurate optical imaging of the connected droplets in addition to electrical measurements of bilayer capacitance, and it allows for reversibly varying bilayer area. After validating the accuracy of the technique with diphytanoyl phosphatidylcholine (DPhPC) DIBs in hexadecane, the method is applied herein to quantify separately the effects on membrane thickness and tension caused by varying the solvent in which the DIB is formed and introducing cholesterol into the bilayer. Because the technique relies only on capacitance measurements and optical images to determine both thickness and tension, this approach is specifically well-suited for studying the effects of peptides, biomolecules, natural and synthetic nanoparticles, and other species that accumulate within membranes without altering bilayer conductance.

Introduction

Cell membranes are soft materials that play critical roles in physiological processes both by acting as selectively permeable barriers and by providing a two-dimensional, liquid crystalline bilayer in which transmembrane proteins are anchored. The membrane is involved in physiological processes ranging from homeostasis to vesicle trafficking and many other forms of cellular signaling. For these reasons, methods to quantify physical properties of membranes provide direct insight into how their structures impact their functions.

Further, there is increasing evidence that biomacromolecules,[1–3] cell-penetrating peptides[4,5] and nanoparticles,[6–8] and other small molecules such as anesthetics or drugs[9–12] affect the packing and conformations of lipids in the membrane. For example, the bulk hydrophobic region of cholesterol is known to affect the structural order and fluidity of phospholipid bilayers by interdigitating between the acyl chains of neighboring lipids.[13–17] And because the interactions between lipid bilayers and cholesterol, transmembrane proteins, and membrane active pharmaceuticals can alter the tension of the membrane, methods for quantifying membrane tension can be applied to study the uptake and accumulation of a variety of important species into lipid bilayers.[1]

Motivated by many of the same reasons described above, scientific literature has produced several methods for measuring tension in synthetic model membranes known as lipid bilayers or black lipid membranes (BLM).[18–20] In many of these studies, the lipid bilayer was formed by spreading a lipid–oil mixture across a small aperture in a hydrophobic solid support submerged in water.[18,20] As illustrated in Fig. 1A, the suspended BLM consists of the thinned bilayer region of the painted film, which is stabilized at its perimeter by an annulus of excess solvent. It is well known that the bilayer region and the annulus reach mechanical equilibrium through a balance of surface tensions, obeying Young's equation:[21–24]

[a] *Mechanical, Aerospace, and Biomedical Engineering, University of Tennessee, 1512 Middle Drive, 414 Dougherty Engineering Building, Knoxville, TN 37996, USA. E-mail: ssarles@utk.edu*

[b] *Center for Nanophase Materials Sciences, Oak Ridge National Laboratory, Oak Ridge, TN 37831, USA*

† Electronic supplementary information (ESI) available: Droplet deformation and area calculation, pendant drop method details, uncertainty and error in tension measurements, mechanical manipulation and electrowetting, measuring voltage-dependent C_M. See DOI: 10.1039/c5sm01005e

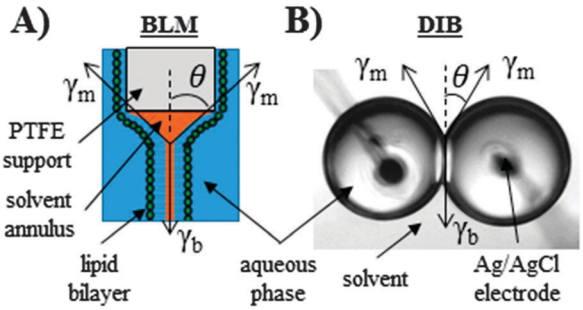

Fig. 1 Common model membranes include the black lipid membrane (A) and the droplet interface bilayer (B). In both cases, the tension of the lipid bilayer that forms is in equilibrium with the vertical sum of the two opposing monolayer tensions.

$$\gamma_b = 2\gamma_m \cos\theta. \quad (1)$$

Specifically, the interfacial bilayer tension (γ_b) is balanced by the two lipid monolayer tensions (γ_m) at the annulus–water interface oriented away from the plane of the membrane by the contact angle (θ). Knowledge of the contact angle and monolayer tension allows for direct calculation of bilayer tension *via* the Young equation as well as the specific free energy of bilayer adhesion (also known as free energy of formation, ΔF):[18,21–23,25]

$$\Delta F = 2\gamma_m(1 - \cos\theta). \quad (2)$$

Given a number of established methods for measuring monolayer tension (*e.g.* drop volume, pendant drop, Wilhelmy plate, *etc.*), the most difficult aspect of determining bilayer tension in a suspended BLM is obtaining an accurate measurement of the contact angle at the annulus.

Requena, Needham, and Haydon[18,20] pioneered specialized techniques to measure the contact angle of suspended BLMs such that they could combine them with monolayer tension values obtained from separate drop volume experiments to calculate the interfacial tensions of glycerol monooleate and phospholipid bilayers.[18,20] *Via* their technique, BLM contact angle measurements are made after introducing a lens of excess solvent into thinned lipid bilayer. Requena and Haydon's measurements of contact angle relied on imaging the concentric fringe patterns (visible rings created by constructive and destructive interference) cast by transmitted light passing through the solvent lens,[20] while Needham and Haydon imaged the lens directly to compute θ from the geometric relationship between the radius and volume of the lens.[18] In both cases, bilayer tension was computed using Young's equation by combining contact angles measured *in situ* with monolayer tension values obtained *a priori via* the drop-volume method. The approach is sufficiently quantitative, however, separate equipment and multiple experiments are required to determine monolayer and bilayer tensions. A method that provides simultaneous access to both monolayer tension and contact angle would thus enable *in situ* measurement of lipid bilayer tension and determination of free energy of formation.

Petelska *et al.* presented a different approach for measuring BLM tension, which they used to study the effects of cholesterol,[1,26] charged lipids,[2] pH,[19] and the presence of amino acids on the tension state in membranes.[19] Petelska's method of bilayer tension measurement involves forming a planar bilayer and applying a differential hydrostatic pressure across the membrane, such that the Young–Laplace equation ($\Delta P = 2\gamma_b/R$) could be used to determine bilayer tension from the radius of curvature of the bulging bilayer.[19] The Young–Laplace equation relates the pressure differential to the radius and tension of the bilayer only. Thus, one drawback of this technique is that it does not allow for direct determination of contact angle, monolayer tension, or free energy of formation.

It is well known that applying voltage across a BLM affects the equilibrium interfacial geometry of the suspended film through a process known as electrowetting.[20,24,27,28] Specifically, an applied electric field increases the external contact angle at the annulus, which drives a subsequent increase in area of the bilayer. The relationship between the contact angle and the applied electric field is described by the Young–Lippmann equation that relates the change in contact angle at the edge of the bilayer to the specific capacitance of the membrane and monolayer tension. When the membrane specific capacitance and monolayer tension are themselves not functions of voltage, the change in contact angle is described by

$$\cos\theta_0 - \cos\theta_V = \frac{C_M}{4\gamma_m}V^2. \quad (3)$$

Eqn (3) includes the contact angle measured at a nonzero applied voltage (θ_V), the zero-volt contact angle (θ_0), the capacitance per unit area of the membrane (C_M), the monolayer surface tension, and the voltage applied across the membrane (V). Eqn (3) shows that if C_M is known, γ_m can be determined experimentally by measuring the voltage dependent change in the cosine of the contact angle. Requena and Haydon[20] were the first to verify that this relationship could provide access to γ_b, though they suggested that either C_M or γ_m would be known ahead of time from a separate experiment. Their work also highlighted the difficulty in determining an accurate value for the area of a suspended BLM, which is required to precisely determine C_M. Consequently, rather than using eqn (3) to extract monolayer or bilayer tensions, they used this relationship and separate measurements of γ_m as a way to determine C_M from the electrowetting response.[20] This approach contrasts the more commonly used discrete measurements of electrical capacitance and bilayer area to determine specific capacitance.[20,28–45] Yet, if C_M and θ_V can be measured *in situ*, then the Young–Lippmann relationship and Young's equation show that γ_m, γ_b, and the free energy of bilayer formation can be comprehensively and simultaneously determined.

The droplet interface bilayer (DIB) method is an elegant technique for assembling planar lipid bilayers to study membrane properties and membrane protein activity.[27,46–57] Droplet interface bilayers form spontaneously between lipid-coated aqueous volumes immersed in oil. DIBs offer several advantages to other methods for bilayer formation, including long lifetimes (hours-days),[58] low-volume, tunable bilayer area,[24,27,54–56,58,59] control over the composition of each leaflet and of each droplet,[57] and potential for scale-up by forming multi-membrane networks with many droplets.[47–53] DIBs have been successfully used as soft functional building blocks for

bottom-up synthetic biology, for example in the construction of tissue-like materials[48] and in the construction of spatially arranged artificial cells.[60,61] As illustrated in Fig. 1B, a DIB is energetically balanced by lipid monolayer tensions that oppose bilayer tension in the same manner as a suspended BLM. DIBs also possess the appropriate thickness and amphiphilic, two-dimensional liquid crystalline structure to reconstitute transmembrane proteins and peptides while retaining their natural function.[58,62,63] However, unlike suspended BLMs, the DIB allows for optically tracking both the contact angle and the interfacial area between droplets, in addition to permitting electrical measurements of membrane capacitance.

Thus, we propose that DIBs could be employed to study the effects of proteins, cell-penetrating peptides, and other biomolecules and lipophilic species on bilayer capacitance, tension, and free energy of formation by combining methods for determining membrane specific capacitance with a technique to measure contact angle. Using a coupled approach, we demonstrate that both monolayer and bilayer tensions can be measured *in situ* by tracking changes in C_M and θ with a droplet interface bilayer (DIB) at varying bias voltages. The specific advantages of DIBs for this type of experiment include: (1) control of droplet positions relative to one another allows for direct tuning of the area of the interface,[58,59] which allows for accurate determination of C_M,[27,56] and (2) simple optical imaging of the adjoined pair can be used to determine both membrane area and θ across a range of applied electric fields.[22–24]

In the following sections, we demonstrate the accuracy and sensitivity of a multi-step tuning technique that allows for measurement of monolayer and bilayer tension in a DIB. First, mechanical tuning of the interfacial area is used to determine specific membrane capacitance. Then, an electrical tuning routine is performed to determine lipid monolayer tension *via* C_M and θ values obtained at various applied voltages. Bilayer tension is subsequently determined from values of γ_m and θ using eqn (1) (Young's equation). *In situ* measurements of monolayer tension are compared to separate measurements of monolayer tension obtained *via* the pendant drop method. After confirming that monolayer tensions can be accurately obtained *via* measurements of C_M and θ, we showcase the utility of this method for measuring changes in membrane capacitance, monolayer tension, and bilayer tension (*via* the Young's equation) caused by the addition of cholesterol, known to affect lipid packing and order and, separately, the incorporation of silicone oil into the oil phase surrounding the droplets. The ability to detect cholesterol-induced changes in thickness help validate the method for future use in studies of the effects of other biomolecules, while measurements using different mixtures of oils confirms what is known about size-selectivity of oil retention *versus* exclusion in a BLM. These oil mixtures also represent commonly used oils in DIB assembly.[48,64]

Materials and methods

Materials

Sodium chloride (NaCl), 3-(*N*-morpholino)propanesulfonic acid (MOPS), sodium hydroxide (NaOH), agarose (A9539), *n*-hexadecane (99%), AR20 silicone oil (product number 10836), acetone, and isopropyl alcohol (IPA) are acquired from Sigma Aldrich. Aqueous buffer (pH 7.4, 100 mM NaCl, 10 mM MOPS) is prepared as described previously.[56] 1,2-Diphytanoyl-*sn-glycero*-3-phosphocholine (DPhPC) and cholesterol (ovine wool, >98%) are acquired as lyophilized powders from Avanti Polar Lipids, Inc. and stored at −20 °C. To prepare solutions of single unilamellar DPhPC liposomes, lipids are first suspended in aqueous buffer at a concentration of 2 mg mL^{-1} before being subjected to 5 freeze/thaw cycles to create stock solutions of multilamellar liposomes. Unilamellar DPhPC liposomes are formed by extruding thawed stock lipid solution through 100 nm-pore polycarbonate membranes (Whatman) using an Avanti Mini Extruder. To create liposomes containing DPhPC and cholesterol, the lyophilized (powder) form of each component is dissolved in chloroform to create separate 5 mg mL^{-1} stock solutions. Appropriate volumes of each chloroform stock are mixed to obtain the desired DPhPC : cholesterol molar ratio, and the vial containing the mixture is placed under vacuum for several hours to remove the solvent. The resulting films are rehydrated with buffer to achieve a final DPhPC concentration of 2 mg mL^{-1}, incubated between 35–45 °C to help dissolution, and then sonicated at 45 °C using a bath sonicator (FS20D, Fisher Scientific) for several hours or until the solution is completely clear. Sonication is preferred over extrusion with cholesterol-containing mixtures to prevent removal of cholesterol by the polycarbonate membranes during extrusion. Sonicated and extruded liposome solutions are stored at 4 °C until further use. Cholesterol-containing solutions are checked for optical clarity before testing and re-sonicated to clarity if there is any evidence of cholesterol demixing.

Methods for DIB formation and characterization

DIBs are formed between two aqueous droplets suspended in the oil-filled reservoir of a transparent PDMS substrate, as described elsewhere.[56] Briefly, aqueous droplets (300 nL unless otherwise stated) are pipetted onto agarose-coated, ball-end silver/silver-chloride electrodes made from 50 μm silver wire (Sigma). Suspended droplets "hang" on the gel-coated electrode tips under oil and are intentionally free of contact with either the upper oil/air interface or the PDMS substrate. Optical clarity is improved by injecting a small volume (<10 μL) of hexadecane between the substrate and microscope slide. Each electrode is affixed to a 3-axis micromanipulator (World Precision Instruments, Kite-L and Kite-R models) to allow precise control over the position of each droplet. To dynamically vary bilayer area when determining specific capacitance, one droplet is moved closer to or further away from the other droplet using the micromanipulator. Current measurements are made using an Axopatch 200B patch clamp amplifier and Digidata 1440 data acquisition system (Molecular Devices). All recordings are made with appropriate shielding in place to reduce noise to less than ±5 pA. Nominal capacitance measurements are based on the bilayer's current response to a 10 mV, 10 Hz triangular voltage waveform output from an Agilent 33210A waveform generator.[56] Membrane capacitance is extracted from sections of the square-wave current response

using MATLAB. To induce electrowetting between droplets, custom dc step voltage routines are employed as described previously.[56] Images of DIBs taken from below through the 4× objective lens of an Olympus IX50 inverted microscope are acquired with a QI Click CCD camera controlled using μManager software.[65] DIB images are post-processed using custom scripts in MATLAB to extract bilayer contact length (used for bilayer area calculation) and contact angle (for measurements of tensions and free energies). Bilayer area calculations account for droplet sagging due to differences in density between the aqueous and oil phases (refer to ESI† for details). In every DIB test, we carefully ensure droplets are freely suspended under oil and above the substrate surface to reduce error in our calculation of bilayer ellipticity. Practically, an important aspect of measuring DIB length is that the droplets are positioned at the same height such that the waist of each droplet is in focus when viewed from the bottom-up. The height of each droplet is adjusted before specific capacitance and tension measurements to maintain appropriate focus.

Pendant drop measurements of monolayer tension

Interfacial tension of lipid and lipid–cholesterol monolayers formed at various oil–water interfaces are measured *via* the pendant drop method with a Model 590 goniometer and DROPimage Advanced software (Ramé-Hart Instrument Co.). The method involves forming a pendant drop from one of the liquid phases (*i.e.* aqueous solution) at the tip of a needle submerged in the other phase (*i.e.* oil). A horizontally mounted camera acquires images of the droplet profile at a frequency of 1 Hz, which are used by the software to compute the surface tension *versus* time. Refer to the ESI† for additional details regarding pendant drop measurements.

Results and discussion

I. Specific capacitance, monolayer tension, and bilayer tension measurement with a DIB

Fig. 2A illustrates the three-part process for measuring C_M, γ_m, and γ_b on a DIB. In Part 1, a DIB is formed between two aqueous droplets suspended on agarose tipped ball-ended electrodes in oil. The initial thinning of the bilayer occurs generally within 1–2 minutes of initial contact and results in a rapid increase in the amplitude of the capacitive current signal due to the formation of a thinned bilayer region between droplets. The area of the thinned region and the angle between droplets stabilize to constant values when the total energy of the connected droplets reaches a local minimum.[48]

Part 2 of the process involves incrementally changing the bilayer area, and thus the nominal capacitance of the interface, by moving one electrode in a stepwise fashion relative to the other. As others have shown,[27] returning the mobile electrode to its original position results in a reversible change in the capacitive current and bilayer area. The size of the bilayer at each position stabilizes within about 30 s of the electrode positioning. At each level of contact area (typically >5 contact areas are prescribed), the steady-state amplitude of the square-waveform current signal is recorded and an image of the DIB is acquired simultaneously. Nominal capacitance is computed using $C = i/(4Af)$, where i is the amplitude of the current waveform measured at steady state and A and f are the amplitude and frequency, respectively, of the applied triangular waveform voltage. Specific capacitance is obtained simply from the slope of a linear least squares regression of nominal capacitance *versus* area data from all electrode positions (Fig. 2A, center).[27,56]

Part 3 requires an applied dc transmembrane voltage that increases in a stepwise fashion in addition to the ac triangular voltage required for capacitance measurement. This procedure begins by fixing the electrode (*i.e.* droplet) positions, setting the bias voltage to zero, and allowing the DIB to equilibrate for several minutes to ensure the droplets reach a steady contact area and angle. Images are taken at the 0 mV equilibrium point to allow measurement of θ_0 before voltage is increased in a stepwise fashion. The bilayer is held at each new voltage for 15–30 seconds, during which electrowetting causes the external bilayer contact angle to increase as predicted by the eqn (3) (Young–Lippmann equation). Images ($n \geq 10$) of the contact angle (θ_V) are obtained at the end of each voltage step and the process is repeated at successively higher voltage levels. This part of the experiment takes only a few minutes to perform. Using the average contact angle from each voltage level, the change in the cosine of the contact angle is plotted *versus* the square of the applied bias voltage (Fig. 2A, right). As noted above with eqn (3), the change in the cosine of the contact angle is recorded with respect to the cosine of θ_0.

Fig. 2B shows the square current waveform induced by the ac triangular voltage applied to a DPhPC DIB formed in hexadecane during all three parts of the experiment. Fig. 2C shows the corresponding bilayer capacitance, computed from the same current response, *versus* time. During Part 1 of the experiment, the amplitude of square current waveform stabilizes at $\sim$240 pA. Images of the connected droplet pair show that θ_0 is 29.3° for this type of lipid and oil.

The second and third parts of the measurement process result in stepwise changes to bilayer capacitance, caused by mechanical and electrical tuning, respectively. During Part 2, the measurement shows that at each successive electrode position (*i.e.* farther apart), the square wave current stabilizes to smaller amplitude, which corresponds to smaller area of contact and thus capacitance. Conversely, the application of an increasing dc bias (of either polarity) drives the square wave current and bilayer capacitance to successively higher levels in Part 3.

The micrographs of a DPhPC DIB in decane in Fig. 3A show that increasing levels of electrowetting lead to increases in the external contact angle, θ, as well as the projected length of the interface, a. Fig. 3B presents the capacitance *versus* area data obtained in Part 2 of a test with a DPhPC DIB in hexadecane, and the change in the cosine of the contact angle *versus* voltage data from Part 3 are shown in graphical form in Fig. 3C. Typically, tests to measure γ_m conclude when the bilayer ruptures at voltages between |200–350| mV. In this test, θ

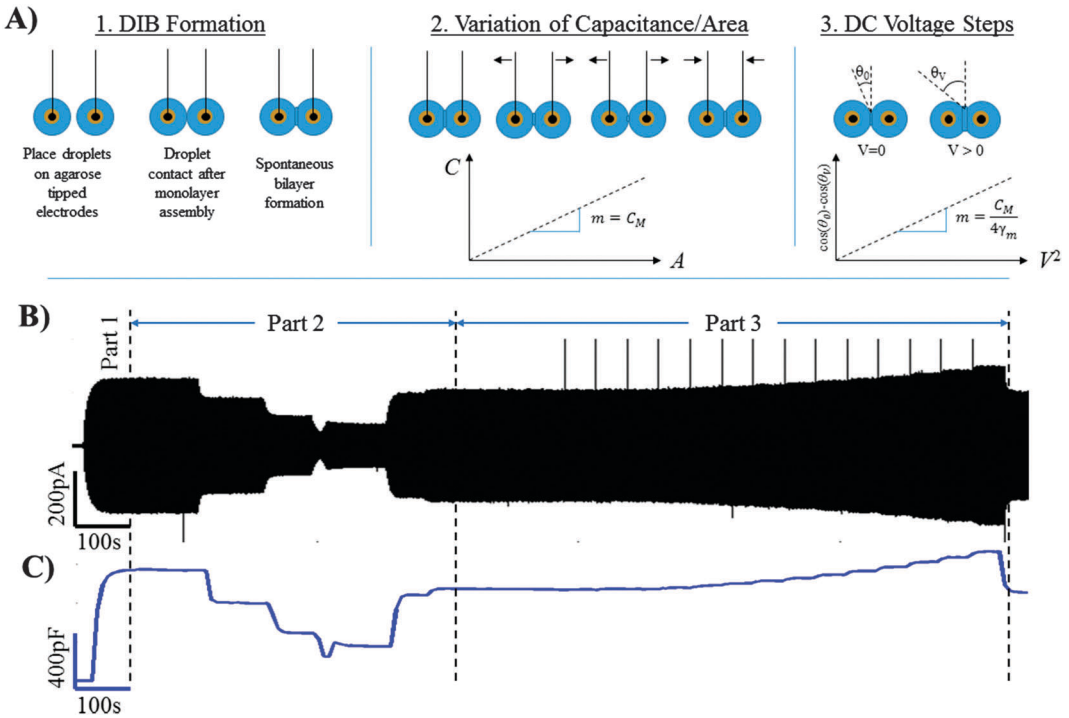

Fig. 2 (A) A three-part process is used to characterize DIBs: Part 1 represents bilayer formation; Part 2 represents the mechanical tuning of the bilayer area to determine specific capacitance; and Part 3 represents electrical tuning of the contact angle to determine monolayer tension *via* the Young–Lippmann equation (eqn (3)). (B) A typical current trace recorded during the course of an experiment in which all three parts are performed. (C) Membrane capacitance *versus* time computed from the raw square current waveform shown in (B).

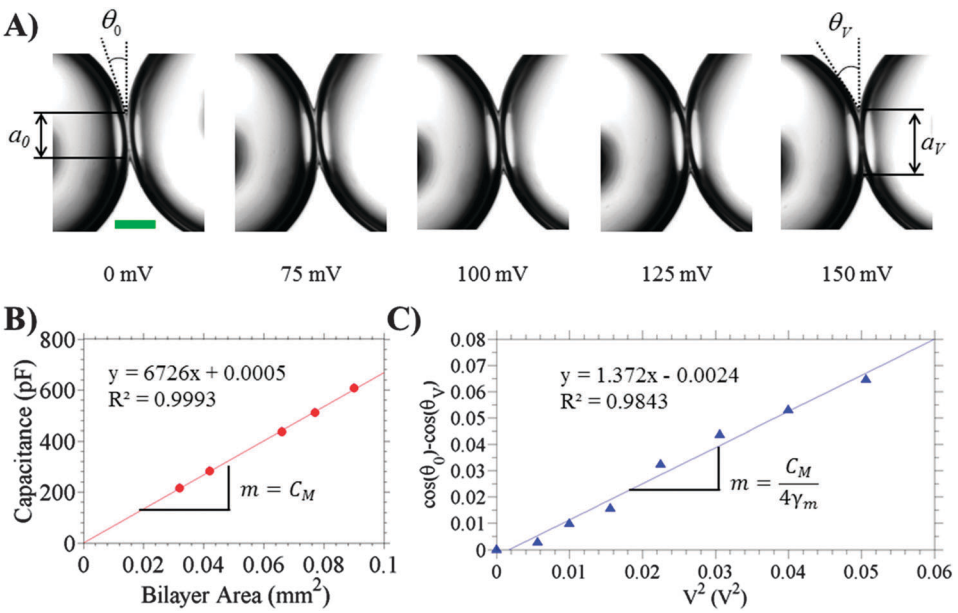

Fig. 3 (A) Representative images of a DPhPC DIB in decane during a Young–Lippmann test for monolayer and bilayer tensions (bottom-view images, scale bar represents 100 μm). The DIB is allowed to equilibrate at each voltage before capturing any images used for contact angle measurements. The contact angle and the contact area increase with increasing voltage. This behavior is a result of reduction in bilayer surface tension by an amount equal to the energy stored on the capacitor. (B) Results from specific capacitance measurement (V = 0 mV, Part 2 in Fig. 2). (C) The Young–Lippmann equation describes the linear relationship between applied bias voltage and the resulting change in the cosine of the contact angle. Experimental observation of contact angle at various applied voltages then allows for calculation of the monolayer tension. Parts B and C represent data obtained from a DPhPC DIB in hexadecane.

increased from 28.8° at 0 mV to 35.9° at +225 mV. The change in cosine of the contact angle is well represented by a linear least squares regression with respect to V^2 across the range from 0 to 225 mV with an R-squared value >0.98. From eqn (3),

it can be seen that the slope of the regression (m) is related to both C_M and γ_m, as given by

$$m = \frac{C_M}{4\gamma_m}. \quad (4)$$

Eqn (4) is rearranged to solve for monolayer tension using the value of C_M obtained in Part 2 and the value of m obtained in Part 3. The specific data shown in Fig. 3C yield a slope of m = 1.372 which, combined with the C_M value (slope from Fig. 3B) of 0.673 μF cm^{-2}, yields a computed value of monolayer tension, γ_m, equal to 1.23 mN m^{-1}. For a group of eight DPhPC DIBs formed in hexadecane, this method results in an average (±one standard deviation) monolayer tension of 1.18 ± 0.136 mN m^{-1}, which is in excellent agreement with prior results[25] and the results of our own independent pendant drop measurements of DPhPC monolayer tension (1.19 ± 0.067 mN m^{-1}, n = 3). A student t-test confirms that there is no significant difference ($p < 0.005$) between the values obtained with either tension measurement method, which serves to validate an approach that leverages the electrowetting response of DIBs to determine the tension state. In summary, the measurement method introduced herein is capable of determining lipid monolayer tensions at the surfaces of the droplets that are consistent with those obtained using accepted techniques such as pendant drop goniometry.

After computing monolayer tension, the bilayer tension at zero volts is readily computed for each trial using Young's equation (eqn (1)) along with the measured contact angle at 0 mV.[18,21,66] For the example shown in Fig. 3, the calculated monolayer tension (1.23 mN m^{-1}) and zero-volt contact angle of 28.8° results in a calculated value for γ_b of 2.16 mN m^{-1}. For the pool of eight different DPhPC DIBs in hexadecane that are tested, we obtain an average value of 2.04 ± 0.222 mN m^{-1} for the tension of DPhPC bilayers in hexadecane. Prior studies obtained values of 1.62 mN m^{-1} and 1.9 ± 0.3 mN m^{-1} for planar lecithin bilayers[19,67] and DPhPC DIBs,[25] respectively. The latter value, provided by Dixit *et al.*, was obtained using eqn (1) along with the monolayer tension determined *via* independent goniometer measurements and the contact angle estimated using images of connected droplets. It is possible to calculate bilayer tension *via* eqn (1) using the data herein: the average value of monolayer tension obtained from the goniometer and the average contact angle in DIB measurements (29.3°, see Table 1) yields an estimate of 2.08 ± 0.198 mN m^{-1} for bilayer tension. All of these results are in strong agreement with one another, and there is no significant difference ($p < 0.005$) between bilayer tensions computed from monolayer tensions obtained *via* the pendant drop and DIB methods.

It is also possible to use eqn (1) to discretely compute bilayer tension as a function of bias voltage using the measured values of γ_m (fixed) and DIB contact angle at each voltage applied during Part 3 of the experiment. Additionally, the average bilayer tension can be empirically projected in a continuous fashion *versus* voltage using experimentally determined values of C_M, γ_m, and θ_0. This second method evaluates bilayer tension *versus* voltage using a rearranged form of eqn (3),

$$\gamma_{b,V}(V) = \gamma_{b,0} - \frac{C_M}{2}V^2, \quad (5)$$

along with the bilayer tension at 0 mV ($\gamma_{b,0}$) computed using eqn (1). Fig. 4 compares γ_b as a function of voltage computed discretely and continuously using the values of θ, C_M, γ_m, and V obtained for the data presented in Fig. 3B and C. Clearly, γ_b decreases with increasing voltage, which illustrates that the stored electrical energy across the bilayer acts to mechanically relax the interface. Further, close agreement between the

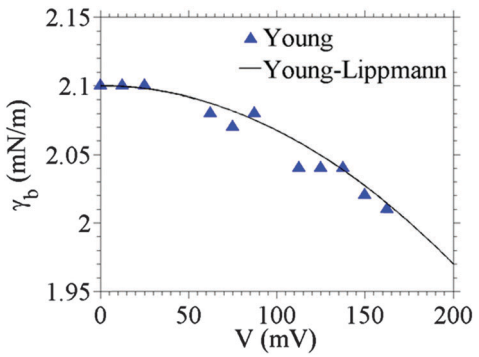

Fig. 4 Bilayer tension (γ_b) as a function of applied voltage (V) for a DIB, calculated using the representative data presented in Fig. 3.

Table 1 Values obtained for DIBs formed at 25 °C

Lipid type	C_M [μF cm^{-2}]	D_C [Å]	γ_m [mN m^{-1}] [a]	γ_m [mN m^{-1}] [b]	γ_b [mN m^{-1}]	$\theta_{0,eq}$ [°]	ΔF [mN m^{-1}] [mJ m^{-2}]
DPhPC hexadecane	0.652 (0.027) n = 13	29.9	1.18 (0.136) n = 8	1.19 (0.067) n = 3	2.04 (0.222) n = 8	29.31 (2.13) n = 116	0.302
DPhPC, 1 : 1 AR20 : hex	0.667 (0.022) n = 9	29.2	1.03 (0.115) n = 4	1.01 (0.041) n = 3	1.54 (0.198) n = 4	41.63 (2.21) n = 37	0.520
DPhPC, 9 : 1 AR20 : hex	0.701 (0.027) n = 9	27.8	—	—	—	42.15 (7.39) n = 84	—
DPhPC, decane	0.488 (0.043) n = 7	39.9	1.09 (0.095) n = 7	—	2.11 (0.173) n = 7	15.40 (1.06) n = 43	0.078
DPhPC, 20% Chol. hexadecane	0.655 (0.030) n = 8	29.7	1.42 (0.051) n = 6	1.40 (0.111) n = 3	2.50 (0.095) n = 6	27.10 (1.65) n = 80	0.312
DPhPC, 20% Chol. 1 : 1 AR20 : hex	0.713 (0.045) n = 3	27.3	1.24 (0.056) n = 4	1.15 (0.045) n = 3	1.92 (0.056) n = 4	38.85 (2.34) n = 128	0.548

[a] DIB-electrowetting/Young–Lippman method. [b] Pendant drop with goniometer. —: not measured. D_C: hydrophobic thickness, $D_C = (\varepsilon_r\varepsilon_0)/C_M$.

discrete data points and the continuous curve show that the measured contact angles and thus the computed bilayer tension, conform to the Young–Lippmann relationship for bilayer tension at voltages between |0–175| mV. This agreement suggests that bilayer tension can also be computed accurately at a non-zero voltage provided the contact angle is measured at that potential and the monolayer tension is known. Monolayer tension is assumed to be independent of applied potential due to the fact that the thinned bilayer contributes the dominant electrical impedance between droplets. This occurs because of the presence of nonconductive oil in the Plateau–Gibbs border that is much thicker and has a lower capacitance per unit area than the bilayer. As a result, the applied voltage produces an electric field predominantly across the membrane.

For further comparison of the DIB Young–Lippmann equation with prior studies, it is possible to evaluate the reduction in free energy obtained upon droplet adhesion (eqn (2)). For a DPhPC DIB formed in hexadecane, the calculated monolayer tension and average contact angle at 0 mV (29.3°) yield 0.301 mJ m^{-2} as the free energy of bilayer formation. As further validation of the accuracy of the approach, our estimated free energy of formation is in direct agreement with the value of 0.31 ± 0.02 mN m^{-1} for DPhPC bilayers formed in squalene,[23] as well as other reported values which fall between 0–2 mN m^{-1}.[18,21,22,25]

Uncertainty of capacitance and tension measurements. Error in determining specific capacitance and tensions arises from uncertainties in measuring capacitance and area (for C_M) and in determining the contact angle (for γ_m, γ_b), respectively. Nominal capacitance is determined directly *via* electrical measurement as described previously[56] where it is shown that there is $<1.3\%$ error in any *C versus A* data point used for C_M determination.[56] Therefore, we focus instead on the accuracy and repeatability of bilayer area and contact angle measurements, which are obtained *via* a two-step process: (1) an image acquisition step, and (2) image processing (MATLAB) to determine the angle and projected length (diameter) of the bilayer. To determine uncertainties introduced from image acquisition, we look at repeatability of measurements taken from 10 images of a DIB at a fixed equilibrium condition. The images are acquired rapidly within a few seconds. Estimation of bilayer area begins in MATLAB by extracting the projected diameter of the bilayer from images taken through the inverted microscope objective. These "bottom-view" images are analyzed *via* a custom image processing routine to calculate the horizontal distance, a, between the intersection points of the two droplets and the external half angle (*i.e.* contact angle), θ, that exists at the waist of the interface (as shown in Fig. 3A). Area estimation requires an assumption regarding the shape of the interface. Dixit *et al.* outlined the geometrical relationships that govern DIB formation for spherical droplets of identical size in an equally dense oil phase. This analysis predicts a perfectly flat, circular interface.[25] However, the shape of the interface becomes more elliptical when gravitational effects cause the water droplets to sag vertically from the wire-type electrodes in a less dense oil phase (refer to ESI,† Fig. S4). With droplets hanging on electrodes, the minor axis of the elliptical interface (a) is the horizontal distance obtained from microscope images whereas the longer major axis (b, ESI,† Fig. S4) is oriented vertically and cannot be determined from a bottom-view image. Analysis of bilayer shape under increasing levels of sagging enables estimation of correct bilayer area using only a. However, since the contact angle is measured in the horizontal plane at the waist of the connected droplet pair (*i.e.* the force balance at the contact point does not have a vertical component), we do not correct the measured contact angle for effects of droplet sagging.

The average and standard deviation of bilayer area and contact angle are calculated from the 10 images acquired with zero applied voltage to assess the repeatability. Furthermore, the average group standard deviation of bilayer area using images acquired from 11 unique DPhPC bilayers (110 images total) is 458 μm^2. Similarly, contact angles measurements from 14 different DPhPC DIBs (140 images total) provide an average group standard deviation of only 0.763°. With a typical zero-volt area of 30 000 μm^2 for a DPhPC DIB in hexadecane, the average standard deviation in measured bilayer area corresponds to an error of less than 0.002%. For the average contact angle of 29.3°, the average standard deviation represents an error of 2.6% for the angle measured at a given area step. These results present a lower standard deviation than previously reported for contact angle measurements in DIBs (σ = 3–6°) in DIBs.[22,23] The comparison here shows that the automated image processing routine and the use of multiple images at each voltage level provide an order of magnitude lower variation in average angle measurements. Separate analysis for quantifying error propagation within the multi-step technique (refer to ESI† for additional details) yields uncertainties of ±0.32 mN m^{-1} and ± 0.51 mN m^{-1} in monolayer and bilayer tension measurements, respectively.

Effects of mechanical manipulation on electrowetting and tension measurements. In analyzing images obtained during specific capacitance measurements of DIBs (Fig. 2A, Part 2), we observe that the zero-volt contact angle at equilibrium is directly affected by mechanical manipulation (*i.e.* positioning) of the droplets, which is used to intentionally vary the area of the bilayer. To explore this relationship, Fig. 5A and B shows the results of a representative experiment in which droplets supporting a DIB were successively pulled apart in 3 steps and then sequentially pushed back together in 3 area steps (refer to Fig. S7 in the ESI† for sequential presentation of area and angle data). The data in Fig. 5B shows that the contact angle reversibly increases by as much as 5–6° as 300 nL droplets are pushed together to yield a larger interfacial area. To further test this response, Fig. 5C shows zero-volt contact angle *versus* bilayer area obtained from n = 115 various measurements made *via* Part 2 of the method on 13 different DPhPC DIBs. The larger population of data confirms that contact angle increases with mechanically driven increases in bilayer area. While the precise mechanism for this change in angle remains undetermined, the data suggest that pushing or pulling the droplets in a direction perpendicular to the interface reversibly alters the equilibrium tension balance that establishes the contact angle.

The fact that changing the electrode separation distance alters droplet contact angle begs the question: how much does mechanical manipulation required for Part 2 affect the accuracy of the

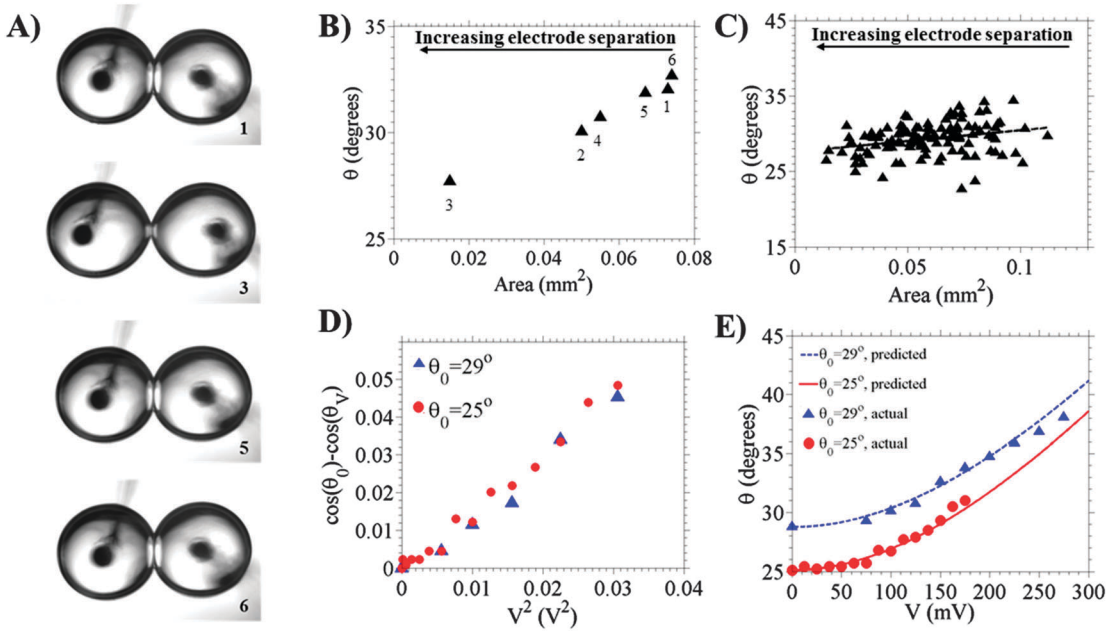

Fig. 5 (A) A DPhPC DIB at varying steps during Part 2 of an experiment where DIB area is mechanically varied by moving one electrode and changing the distance between droplets. (B) θ measured from images of the DIB at each area step. (C) θ measured from $n > 100$ images obtained at varying area steps with 13 separate DPhPC DIBs during C_M measurements. (D) The change in the cosine of θ as a function of voltage for a DPhPC DIB mechanically manipulated to obtain two different zero-volt contact angles: θ_0 = 29° and 25°. (E) Theoretical ("predicted") and experimentally observed ("actual") nominal θ as a function of voltage for the trials shown in (D).

electrowetting-based method in Part 3 for determining monolayer tension in a DIB? To examine this possibility, we consider the role of the zero-volt starting contact angle, which was shown in Fig. 5A and B to be a function of droplet positioning. Based on eqn (3), tuning or altering the initial wetting condition (θ_0) should not affect the magnitude of the change in the cosine of the contact angle across a range of voltage assuming fixed C_M and γ_m. However, the nominal change in contact angle does depend on θ_0 since the cosine of an angle varies nonlinearly. Such behavior is observed experimentally as portrayed in Fig. 5D and E, which show the theoretical and experimentally observed values for $\cos(\theta_0) - \cos(\theta_V)$ and θ_V, respectively, with increasing applied voltage. The data portrayed is from two different electrowetting trials where the zero-volt contact angle is varied (θ_0 = 29° and θ_0 = 25°) by mechanical manipulation between trials. The data in Fig. 5D provides slope values of m = 1.548 and m = 1.579. With a specific capacitance value of 0.652 μF cm^{-2}, the resulting calculated monolayer tensions are 1.05/1.03 mN m^{-1} for (θ_0 = 29°/25°) and the Young equation is used to calculate bilayer tension of 1.84/1.87 mN m^{-1}. The variation in θ_0 causes <2% change to the slope, monolayer tension, and bilayer tension. Thus while mechanical manipulation can affect the zero-volt contact angle, it does not significantly affect the ability to correctly determine monolayer and bilayer tension in the electrowetting-based method used in Part 3.

While varying θ_0 does not affect the magnitude of the change in the cosine of the contact angle, the magnitude of the nominal voltage-dependent change in angle is expected to increase with decreasing zero-volt contact angle due to the nonlinearity of the cosine function (refer to ESI,† Fig. S8). This behavior is seen with both predicted and experimentally observed values for θ_V shown in Fig. 5E, which show that contact angles for DIBs starting at different contact angles appear be on converging trajectories at increasing voltage. These data also confirm that DIB contact angle follows the Young–Lippmann equation up to 175 mV, regardless of starting angle. At higher voltages, the data obtained from the DIB with θ_0 = 29° indicates that the change in the contact angle saturates. The saturation issue will be discussed later, but the immediate point to be made is that the lower initial θ_0 incurs a larger nominal angle change as voltage increases. Thus, while a given amount of electrical energy (for fixed values of V, C_M and γ_m) produces a fixed change in the cosine of the contact angle, the corresponding change in the nominal value of θ is greater when starting from a lower θ_0 (closer to unity on the cosine curve, refer to ESI,† Fig. S9). Because we demonstrated that our method for measuring monolayer and bilayer tensions in a DIB is limited most by the resolution of contact angle measurement, the nonlinear relationship between angle change and applied voltage suggests that achieving a small θ_0 (*e.g. via* mechanical manipulation or even through oil selection) could be used to maximize the nominal change in contact angle and improve the accuracy of this technique. This approach is also common to other electrowetting-based applications, including single droplet electrowetting on dielectric (EWOD) experiments,[68] where tuning the initial wetting condition to make θ_0 small can be used to enhance angle change in response to voltage.[68]

Nonetheless, it is necessary to remember that the nominal contact angle is used in the Young equation to compute bilayer tension. Thus, while the two membranes characterized in Fig. 5D and E exhibited bilayer tensions within 2% of each

other, the amplitude of error in determining bilayer tension also varies nonlinearly with starting contact angle. Thus, it is advisable to initiate Part 3 of the method at a location where the droplets are minimally deformed by electrode separation in order to reduce the effects of mechanical manipulation on the accuracy of determining bilayer tension.

For completeness, we also investigated the effect of starting contact angle on the voltage-induced change in membrane capacitance (refer to ESI,† Fig. S10). This analysis showed that the sensitivities of nominal bilayer capacitance and area to voltage are affected by the starting angle. However, the linear relationship between capacitance and area (Fig. 3B), and thus the determination of C_M, holds across a wide range of areas obtained *via* mechanical manipulation as we[56] and others[27] have shown previously. In a following section we examine if specific capacitance varies under an applied dc voltage.

Limits of electrowetting in DPhPC DIBs. Numerous studies of electrowetting have shown that the change in the wetting angle saturates at high voltage, falling short of the expected angle change predicted by the Young–Lippmann equation.[68–71] With a single sessile droplet placed on a dielectric, common in many EWOD systems, the saturation limit is believed to be the result of dielectric charging or breakdown, charging of the insulating fluid surrounding the droplet, formation of instabilities and/or microdroplet ejection, or reduction of interfacial tension to zero.[69] The zero-tension theory, which states that the maximum angle change occurs at a voltage where the interfacial tension is zero,[69,71] is capable of predicting the saturation angle for single droplet EWOD cases.[69] Applying this concept to a DPhPC DIB, the Young–Lippmann equation predicts that an applied voltage of nearly |800| mV is required to reduce a bilayer tension to zero (calculated using eqn (5) and values of C_M and $\gamma_{b,0}$ for DPhPC DIBs in hexadecane, Table 1). However, because the typical rupture potential of DPhPC DIBs occurs at |200–300| mV,[56] it is unlikely that saturation of the contact angle could be caused by reducing tension to zero. Rather, the observed contact angle saturation at voltages above |175| mV is likely due dielectric breakdown and electroporation which typically precede bilayer rupture.[56,72]

Effect of increasing voltage on C_M. When using specific capacitance to determine monolayer tensions in eqn (3), it is important to understand how much C_M varies when an electric field is applied to induce changes in the contact angle. The effect of voltage on C_M has been shown previously to follow the experimental relation[27,32,40]

$$C_M = C_{M,0}(1 + BV^2), \quad (6)$$

which involves the specific capacitance at 0 mV ($C_{M,0}$), the magnitude of applied dc bias (V), and a parameter (B) describing the voltage dependence of C_M. While electrostriction of the membrane is a possible mechanism for voltage affecting C_M, prior works have shown that planar lipid bilayers formed in the presence of solvents can exhibit voltage-dependent specific capacitance due to the electric field exerting a compressive force that excludes trapped oil from the membrane, thereby reducing the thickness of the hydrophobic core.[27,32,40] This effect is particularly significant when membranes are formed in the presence of organic solvents with high solubility in the hydrophobic region of the bilayer, and less in "solvent-free" membranes formed in the presence of large-molecule solvents that are more easily excluded from the hydrophobic region.[18,73,74]

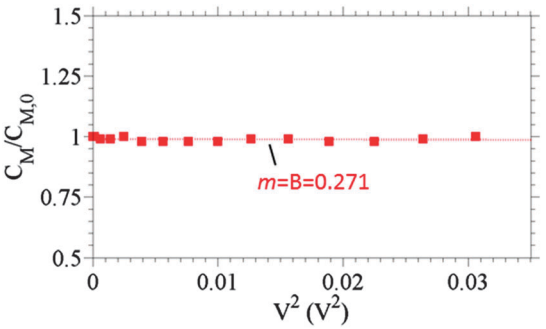

Fig. 6 Normalized specific capacitance for a DPhPC DIB (hexadecane oil phase) as a function of applied voltage. $C_{M,0}$ is the specific capacitance measured *via* dynamic capacitance/area changes with voltage clamped at 0 mV (see Fig. 2, part 2).

Fig. 6 shows values obtained for C_M normalized by $C_{M,0}$ at each voltage step with a DPhPC DIB in hexadecane. Discrete values of C_M at each voltage step are calculated (refer to ESI,† Fig. S11) using the capacitance and area at that voltage step (as opposed to dynamically varying area at each voltage step to determine C_M). Slight nonzero offset (Fig. S11, ESI†) in the total measured capacitance is obtained from mechanical tuning and is used to correct the instantaneous calculated C_M. From eqn (6), linear least squares regression of $C_M/C_{M,0}$ as a function of V^2 yields a straight line with an intercept of 1 and a slope of 0.27 V^{-2} representing the value for parameter B. The resulting value of B indicates that C_M would only increase by 0.01 μF cm^{-2} at a voltage of |200| mV, a deviation that is approximately 1.6% of the value of specific capacitance measured at zero volts for DPhPC DIBs in hexadecane (0.67 μF cm^{-2}). Compared to the larger B values measured for planar bilayers formed with decane as the oil-phase (4 V^{-2}),[27] our result is much lower as expected due to the decreased solubility of hexadecane in the bilayer. Our results are agreement with previously reported values of B in tests with solvent-free supported bilayers.[20,27,41] As a result, small values of B in solvent-free membranes allow for monolayer and bilayer tensions based on contact angle and specific capacitance to be accurately determined using a value of specific capacitance obtained with zero bias applied. This approach is supported by previous reports that the Young–Lippmann equation accurately predicts the response of lipid bilayers subject to applied voltage when using a constant value for $C_{M,0}$.[20,27,75]

II. Application of capacitance and tension measurements

Until now, the multi-part experiment for determining monolayer and bilayer tension has been presented and validated with data obtained from DPhPC DIBs in hexadecane. However, to demonstrate the value of this procedure, we also apply this method to study the effects of oil type and the addition of cholesterol on the specific capacitance and tension state of DIBs. As with DPhPC DIBs in

hexadecane, equilibrium monolayer tensions are compared to values obtained on a pendant drop goniometer.

First, tests are performed to determine monolayer and bilayer tensions for DPhPC DIBs formed in a mixed solvent phase containing silicone oil (AR20) and hexadecane. Prior to performing contact angle measurements *versus* voltage, values of specific capacitance are measured separately for DPhPC DIBs formed in pure hexadecane, in a 1 : 1 (vol : vol ratio) AR20 : hexadecane mixture, and in a 9 : 1 mixture of AR20 : hexadecane. Values obtained for C_M (average ± standard deviation) are shown in Fig. 7A as a function of the volume percentage of silicone oil. These values are then used in calculations of monolayer tension obtained *via* Part 3 of the experiment (Fig. 7B) and are combined with measured values of θ_0 for each to estimate bilayer tension at 0 mV (Fig. 7C). Table 1 presents average values, standard deviations, and the number of trials included for each case tested, as well as for DPhPC DIBs assembled in decane.

It is well established that C_M varies strongly with the amount of solvent in the hydrophobic region.[27,32,73,74] The solubility of solvent in the bilayer region generally increases with decreasing solvent molecule size.[18,73,74] As a result, techniques for measuring the thickness of the hydrophobic region are used to probe the amount of solvent trapped or dissolved in the bilayer.[27,42] C_M is related to the thickness of the hydrophobic region (D_C) and permittivity (ε_r) of the hydrophobic region of the bilayer, as well as the permittivity of vacuum (ε_0) by

$$C_M = \frac{\varepsilon_r \varepsilon_0}{D_C}. \quad (7)$$

The minimum value of C_M for the three oil cases tested is obtained for DIBs formed in pure decane (0.488 μF cm^{-2}), and the result is in close agreement with the value of 0.445 μF cm^{-2} obtained elsewhere.[27] C_M increases by 33% to 0.65 μF cm^{-2} upon changing the solvent from decane to hexadecane, and the result is again consistent with previously reported values around 0.64 μF cm^{-2}.[27,76] Compared to DIBs in hexadecane, C_M increases by 3.1% to 0.67 μF cm^{-2} for 1 : 1 AR20 : hexadecane and by 7.7% to 0.70 μF cm^{-2} for 9 : 1 AR20 : hexadecane, respectively. The increase in C_M with increasing silicone oil in the oil phase indicates a thinner, more solvent-free bilayer, while the reduced value of C_M in decane indicates a thicker, oil-rich bilayer. Assuming a constant dielectric of ε_r = 2.2 for the hydrocarbon-rich hydrophobic region of the bilayer, our values of C_M yield thickness values of 29.9, 29.2, and 27.8 Å for DPhPC DIBs in 1 : 0, 1 : 1, and 9 : 1 mixtures of silicone oil : hexadecane, respectively. The 9 : 1 mixture thus results in bilayers that are 7.3% thinner than those in pure hexadecane. Gross *et al.* reported that the hydrophobic region of DPhPC–hexadecane DIBs is 10% oil by volume, leading us to believe that with DIBs formed in the 9 : 1 mixture, the bilayer hydrophobic region consists of only 2.7% (10–7.3%) solvent by volume. The 1 : 1 mixture invokes a similar effect, although the thickness reduces by only 2.7% leading to hydrophobic regions containing approximately 7.3% (10–2.7%) oil by volume. These estimates assume that the changes in volume, based on C_M measurements, are equal to the changes in membrane thickness (*i.e.* oil distributes evenly across the membrane area and the permittivity is unchanged). Converting percent volume oil to molar volume ratio provides a rough estimate of 6 : 1 for lipids : hexadecane in the hydrophobic region (refer to ESI† for calculation details). The average thickness of DPhPC DIBs in decane is 39.9 Å. Based on the calculated thickness values, DIBs formed in decane are 33.4% thicker than those formed in hexadecane as a result of the increased solubility of small decane molecules in the hydrophobic region.[27] DPhPC bilayers formed in decane are expected to contain around 43% (10% + 33.4%) oil by volume which is in close agreement with the estimate of 38% by Gross and Wallace.[27] Conversion of the volume ratio of lipid : decane to a molar volume ratio suggests that there are 1.7 decane solvent molecules for every lipid molecule present (refer to ESI†).

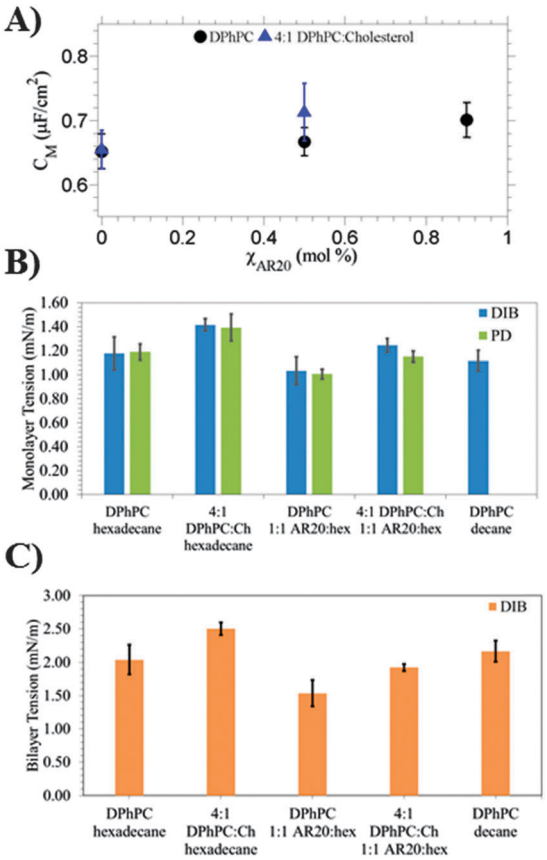

Fig. 7 (A) Values obtained from measurements of specific capacitance for bilayers as a function of the fraction of silicone oil added to the hexadecane oil phase. Error bars show ±one standard deviation. Two lipid compositions are tested in the various oil mixtures: pure DPhPC, and DPhPC containing 20% (mol%) cholesterol. (B) "DIB-YL" – monolayer tensions measured by monitoring Young–Lippmann related changes in DIB contact angle as voltage is increased. "PD" – monolayer tensions measured using the pendant drop method with a goniometer. (C) Bilayer tensions for each lipid–oil combination, calculated using average observed contact angle (case specific) and the monolayer tension measured *via* the DIB-YL method.

In addition to thickness, the oil used to form a DIB affects the tension state of a DIB.[18] Of the oils studied, bilayer tension is highest for DPhPC DIBs formed in decane. The data in Fig. 7 and Table 1 show that the presence of silicone oil has the opposite effect. The average monolayer tension decreases by 17% from 1.18 mN m^{-1} in pure hexadecane to 1.03 mN m^{-1} in the 1 : 1 mixture. Meanwhile, bilayer tension decreases by 29%

from 2.04 mN m^{-1} in hexadecane to 1.54 mN m^{-1} in the 1 : 1 mixture. Note that for 0 : 1 and 1 : 1 AR20 : hexadecane mixtures, the monolayer tension values obtained *via* the multi-step technique introduced herein are not significantly different than the values obtained *via* pendant drop measurements with a goniometer. Tension values are not calculated for DIBs formed in the 9 : 1 AR20 : hexadecane mixture, because these bilayers consistently ruptured at voltages near 100 mV which prevented us from recording the increases in contact angle as applied bias voltage increases.

The free energy of formation is also a metric that can be used to understand the same phenomenon of oil-exclusion. Needham and Haydon[18] and Bibette *et al.*[21,66,77] reported that more solvent-free bilayers exhibit higher free energies of adhesion. Our results show that F is nearly doubled in the 1 : 1 AR20 : hexadecane mixture compared to pure hexadecane, which itself has a F value nearly four times that for decane-rich DIBs. Collectively, the DIB-electrowetting method appears to be a valid approach for measuring γ_m, γ_b, and F, which serve as metrics for detecting solvent the presence of solvent and associated effects on lipid packing. The results of both C_M and F measurements herein support the understanding that addition of AR20 silicone oil to the hexadecane oil phase surrounding the droplets reduces the amount of remaining solvent in a DPhPC DIB, resulting in a thinner, more relaxed interface. The fact that monolayer tension also decreases with increasing silicone oil content, demonstrates that the hydrophobic regions of the lipid tails in monolayer are also better able to exclude silicone oil than pure hexadecane.

In a second study, we applied the multi-step procedure to quantify the effects of cholesterol on C_M and tensions in DPhPC DIBs formed in various organic solvents. We study incorporation of 20 mol% cholesterol and do not pursue higher cholesterol levels due to its reduced solubility in DPhPC bilayers 40 mol% is the maximum for DPhPC,[78] compared with 50–60% across a range of acyl chain compositions (12 : 0, 16 : 0, and 22 : 0) and headgroup types (PC, PG, PE, and PS).[78] When droplets containing DPhPC liposomes with 20 mol% cholesterol are used to form DIBs in pure hexadecane, we obtain a C_M of 0.655 ± 0.030 μF cm^{-2}, γ_m equal to 1.42 ± 0.051 mN m^{-1}, and γ_b of 2.50 ± 0.095 mN m^{-1}. In comparison, DIBs formed in 1 : 1 AR20 : hexadecane from droplets of 20% cholesterol–DPhPC solution yield C_M of 0.713 ± 0.045 μF cm^{-2}, γ_m equal to 1.24 ± 0.056 mN m^{-1}, and γ_b of 1.92 ± 0.056 mN m^{-1}. The results for measured specific capacitance and tensions are illustrated in Fig. 7 and listed in Table 1.

The average value of C_M is higher for DPhPC with 20% cholesterol compared to pure DPhPC in both oil cases tested. Assuming the effective dielectric constant of the interface is unchanged by the incorporation of cholesterol (ε_r = 2.2),[79] eqn (7) shows that the increase in C_M must instead be attributed to thinning of the bilayer hydrophobic region. While numerous studies have identified lipid bilayer thickening upon incorporation of cholesterol,[13–16] the effect depends greatly on the length (relative to cholesterol) and degree of saturation of the lipid being used.[15,17] For instance, McIntosh reports that bilayers comprised of phospholipids with up to 16-carbon acyl chains are thickened by the introduction of cholesterol, whereas 18-carbon chain bilayers in the solid phase (*i.e.* $T < T_m$) exhibit a reduction in thickness upon incorporation of cholesterol.[17] The effects of cholesterol on bilayer thickness are explained by comparing the hydrophobic lengths of the cholesterol and lipid chains.[17] Similar biphasic behavior regarding the effects of cholesterol on lipid transition temperature is also attributed to hydrophobic mismatch.[80] The cholesterol-induced decrease in thickness (Fig. 7A) measured herein suggests that a length mismatch exists between the DPhPC acyl chains and the embedded cholesterol. As encountered by McIntosh with 18-carbon acyl chains, the mismatch between rigid DPhPC tails and cholesterol hydrophobic lengths may create voids near the bilayer mid-plane that prompt the free ends of the acyl chains to bend or kink around embedded cholesterol molecules in an attempt to fill this space. The result is a net shortening of the lipid length and thinning of the bilayer hydrophobic region. This effect is also supported by molecular dynamics simulations showing flexible lipid acyl chains packing tightly around cholesterol molecules.[81]

The fact that C_M increases with the addition of cholesterol in both pure hexadecane and the 1 : 1 AR20 : hexadecane mixture shows that DPhPC bilayers containing cholesterol are thinner than those without cholesterol in each solvent case. Eqn (7) allows calculation of bilayer thickness, again using ε_r = 2.2 as the dielectric constant, which reveals that bilayers containing 20% cholesterol possess a hydrophobic thickness of 29.7 Å or 27.3 Å when droplets are submerged in hexadecane or 1 : 1 AR20 : hexadecane, respectively. Cholesterol reduces the thickness of bilayers in hexadecane by 0.14 Å (<0.5% of nominal value without cholesterol), however when DIBs are formed in a 1 : 1 AR20 : hexadecane oil phase, cholesterol decreases bilayer thickness to 1.88 Å (a 6.4% reduction). This finding is consistent with prior studies that observed increased sensitivity of membrane specific capacitance to small molecules when bilayers are more solvent free, *i.e.* using solvents that are well-excluded from the hydrophobic region.[9,12]

Additionally, our technique allows us to determine that doping a DPhPC bilayer with cholesterol results in an increase in both monolayer and bilayer tension. This result is consistent with the observations of previous studies[67,82] and is explained by the fact that cholesterol interdigitation decreases packing in gel-phase bilayers,[83] such as those formed from DPhPC, which would drive increased interaction between water and the solvent or hydrophobic region of the bilayer. Incorporation of 20% cholesterol increases monolayer and bilayer tension by 0.24 mN m^{-1} and 0.21 mN m^{-1} in pure hexadecane and 1 : 1 AR20 : hexadecane, respectively. The nominal changes to monolayer tension represent a 20.3% spike, while bilayer tension changes by 22.6% or 24.7% in hexadecane or the 1 : 1 AR20 : hexadecane mixture. As with specific capacitance described above, bilayer tension is more significantly affected by cholesterol when the membrane is solvent-free.

Free energy of adhesion (ΔF, eqn (2)) also increases nominally through the incorporation of cholesterol into the bilayer. Raising cholesterol content to 20% increases ΔF of DPhPC DIBs formed in hexadecane by 0.010 mN m^{-1} (+3.3%). For DPhPC DIBs formed in the 1 : 1 AR20 : hexadecane mixture, inclusion of 20% cholesterol causes ΔF to increase by +0.028 mN m^{-1} (+5.4%). It is

interesting to consider the mechanism by which cholesterol increases free energy of adhesion. Evidenced by the equation for free energy (eqn (2)), ΔF increases when either tension or contact angle increase. Our measurements demonstrate the cholesterol increases bilayer and monolayer tensions while causing the contact angle to decrease. To achieve such changes in all three parameters, eqn (1) verifies that the ratio $\gamma_b/2\gamma_m$ must in fact increase in response to the addition of cholesterol. Based on the experimentally obtained values in Table 1, increasing cholesterol content is accompanied by an increase in the ratio of $\gamma_b/2\gamma_m$ (0.853 and 0.880 at 0 and 20% cholesterol, respectively). The data here suggests that cholesterol causes less distortion of lipids positioned in the monolayers around the droplets compared to lipids in the bilayer interface, possibly due to the presence of bulk solvent molecules near the monolayers that fill voids between the sterol and lipid molecules. These results simultaneously support the notion that cholesterol affects bilayer tension more than monolayer tension through the same mechanism that results in membrane thinning: *i.e.* kinking and bending of the lipid acyl chains to "wrap" cholesterol molecules and fill sterol-induced voids in the hydrophobic region.

Collectively, results from our measurements of C_M, γ_m, γ_b, and ΔF confirm that the multi-step process is suitably capable for measuring changes to bilayer thickness and tension caused by changes in membrane composition or oil content. Interestingly, solvent-free DIBs formed in 1 : 1 AR20 : hexadecane displayed a heightened sensitivity in terms of the effects of cholesterol on C_M, D_C, γ_b, and ΔF. These takeaways provide guidance for future studies aimed at investigating the effects of biomolecules, peptides, pharmaceutics, and other species on lipid bilayer thickness and tensions. Specifically, such studies could use 1 : 1 AR20 : hexadecane mixtures to amplify the effects on membrane thickness and tension caused by accumulation of a species of interest.

Conclusions

The Young–Lippmann equation relates changes in contact angle to the applied voltage which affects the interfacial tension. In the DIB platform, where mechanical manipulation can be used to accurately measure C_M, and applied bias voltage induces measurable changes in contact angle, the Young–Lipmann relation provides a framework for simultaneous measurements of both monolayer and bilayer tension. The method is simple and involves measuring changes in the contact angle between droplets as applied bias voltage is increased. Contact angle alone is not sufficient for tension calculations as the Young–Lippmann equation includes membrane specific capacitance. However, specific capacitance is easily and precisely determined during the same test for tensions with droplets suspended on agarose-tipped electrodes. Knowledge of the shape (*i.e.* the circularity) of the interface is crucial to the accuracy of the measurement, particularly in light of observed droplet deformation due to gravity when there is a difference in densities of the oil and aqueous phases. Such density differences are encountered here with $\geq$200 nL droplets in tests using pure hexadecane or mixtures of hexadecane and silicone oil. Further, we learned that the zero-volt contact angle between droplets increases with increasing droplet area (as droplets are pushed together). However, while it was shown that values of monolayer tension are not affected by manipulation-induced changes to θ_0, the nominal contact angle does affect the caculation of bilayer tension In both theory and practice, larger angle changes are obtained for lower θ_0. This conclusion allows tuning of the system (targeting $\theta_0 \leq \theta_{eq}$) to achieve greater angle changes for the same voltage, which increases the signal-to-noise ratio of angle measurement.

With appropriate understanding of the shape of the interface, we demonstrated that this procedure exhibits comparable or better accuracy in measuring values of specific capacitance, bilayer tension, monolayer tension, and free energy of formation to methods described in prior literature. Further, all four physical properties can be measured in a single test over the course of 30 minutes or less. There are several advantages of the DIB-Young–Lippmann approach over supported or painted lipid bilayer techniques:[18,20] (1) forming bilayers between lipid coated droplets allows the area of the bilayer to be easily manipulated, which has been shown to enable accurate determination of specific capacitance and (2) bilayer formation in a liquid environment (*versus* on a solid support) provides direct visual access to bilayer contact length and contact angle.

Measurements of C_M (and thus D_C), γ_b, and ΔF support the conclusion that DPhPC DIBs formed in silicone oil : hexadecane mixtures are more solvent-free than DIBs formed in pure hexadecane or decane. Further, the solvent-free bilayers formed in silicone oil : hexadecane mixtures show an increased sensitivity to the effects of cholesterol on C_M, D_C, γ_b and ΔF. This conclusion suggests that, in future works, tuning oil composition to yield solvent-free bilayers could improve the ability to detect and quantify the effects of biomolecules, nanoparticles, peptides, or other species accumulating in lipid bilayers. The proposed and validated method of measuring capacitance and tensions in a DIB opens the door to being able to study a wide variety of lipidic and non-lipidic species and their effects on membranes. A key application of this procedure is the ability to characterize changes in bilayer physical properties driven by the incorporation of species (*e.g.* cholesterol) that, unlike transmembrane ion channels, do not elicit changes in membrane conductance. The initial embodiment of the method is ready for studies aimed at characterizing, monitoring, or sensing the interactions of a number of small molecules, peptides, pharmaceutic and therapeutic agents, or other lipophilic species with droplet interface bilayers.

Acknowledgements

The authors acknowledge financial support from the Science Alliance Joint Directed Research and Development (JDRD) program and the Air Force Office of Scientific Research, Basic research initiative Grant Number FA9550-12-1-0464. Pendant drop measurements of interfacial tensions of lipid and lipid-cholesterol monolayers were conducted at the Center for Nanophase Materials Sciences, which is a DOE Office of Science User Facility.

References

1 A. Petelska, M. Naumowicz and Z. Figaszewski, *Cell Biochem. Biophys.*, 2006, **44**, 205–211.
2 A. D. Petelska and Z. A. Figaszewski, *Biophys. Chem.*, 2006, **120**, 199–206.
3 A. D. Petelska, M. Naumowicz and Z. A. Figaszewski, *Cell Biochem. Biophys.*, 2011, **61**, 289–296.
4 C. Li and T. Salditt, *Biophys. J.*, 2006, **91**, 3285–3300.
5 Y. Wu, K. He, S. J. Ludtke and H. W. Huang, *Biophys. J.*, 1995, **68**, 2361–2369.
6 R. P. Carney, T. M. Carney, M. Mueller and F. Stellacci, *Biointerphases*, 2012, **7**, 17.
7 C. Leduc, J.-M. Jung, R. R. Carney, F. Stellacci and B. Lounis, *ACS Nano*, 2011, **5**, 2587–2592.
8 A. Verma, O. Uzun, Y. Hu, Y. Hu, H.-S. Han, N. Watson, S. Chen, D. J. Irvine and F. Stellacci, *Nat. Mater.*, 2008, **7**, 588–595.
9 L. Ebihara, J. E. Hall, R. C. MacDonald, T. J. McIntosh and S. A. Simon, *Biophys. J.*, 1979, **28**, 185–196.
10 J. R. Elliott and D. A. Haydon, *Biochim. Biophys. Acta, Biomembr.*, 1984, **773**, 165–168.
11 C. G. Pope, B. W. Urban and D. A. Haydon, *Biochim. Biophys. Acta, Biomembr.*, 1982, **688**, 279–283.
12 J. Reyes and R. Latorre, *Biophys. J.*, 1979, **28**, 259.
13 W.-C. Hung, M.-T. Lee, F.-Y. Chen and H. W. Huang, *Biophys. J.*, 2007, **92**, 3960–3967.
14 F. N. Barrera, J. Fendos and D. M. Engelman, *Proc. Natl. Acad. Sci. U. S. A.*, 2012, **109**, 14422–14427.
15 J. Pan, S. Tristram-Nagle and J. F. Nagle, *Phys. Rev. E: Stat., Nonlinear, Soft Matter Phys.*, 2009, **80**, 021931.
16 N. Kučerka, J. D. Perlmutter, J. Pan, S. Tristram-Nagle, J. Katsaras and J. N. Sachs, *Biophys. J.*, 2008, **95**, 2792–2805.
17 T. J. McIntosh, *Biochim. Biophys. Acta, Biomembr.*, 1978, **513**, 43–58.
18 D. Needham and D. A. Haydon, *Biophys. J.*, 1983, **41**, 251–257.
19 A. D. Petelska, *Cent. Eur. J. Chem.*, 2012, **10**, 16–26.
20 J. Requena and D. A. Haydon, *J. Colloid Interface Sci.*, 1975, **51**, 315–327.
21 A. R. Thiam, N. Bremond and J. Bibette, *Langmuir*, 2012, **28**, 6291–6298.
22 M. Yanagisawa, T.-A. Yoshida, M. Furuta, S. Nakata and M. Tokita, *Soft Matter*, 2013, 5891–5897.
23 S. Thutupalli, S. Herminghaus and R. Seemann, *Soft Matter*, 2011, **7**, 1312–1320.
24 S. Punnamaraju and A. J. Steckl, *Langmuir*, 2010, **27**, 618–626.
25 S. S. Dixit, A. Pincus, B. Guo and G. W. Faris, *Langmuir*, 2012, **28**, 7442–7451.
26 M. Naumowicz, A. D. Petelska and Z. A. Figaszewski, *Electrochim. Acta*, 2005, **50**, 2155–2161.
27 L. C. M. Gross, A. J. Heron, S. C. Baca and M. I. Wallace, *Langmuir*, 2011, **27**, 14335–14342.
28 A. V. Babakov, L. N. Ermishkin and E. A. Liberman, *Nature*, 1966, **210**, 953–955.
29 T. Hanai, D. A. Haydon and J. Taylor, *J. Theor. Biol.*, 1965, **9**, 433–443.
30 S. H. White, *Biophys. J.*, 1970, **10**, 1127–1148.
31 A. Clowes, R. Cherry and D. Chapman, *Biochim. Biophys. Acta, Biomembr.*, 1971, **249**, 301–317.
32 S. H. White and T. E. Thompson, *Biochim. Biophys. Acta, Biomembr.*, 1973, **323**, 7–22.
33 S. H. White, *Biochim. Biophys. Acta, Biomembr.*, 1974, **356**, 8–16.
34 R. Benz, O. Fröhlich, P. Läuger and M. Montal, *Biochim. Biophys. Acta, Biomembr.*, 1975, **394**, 323–334.
35 J. Requena, D. F. Billett and D. A. Haydon, *Proc. R. Soc. London, Ser. A*, 1975, **347**, 141–159.
36 J. Requena and D. A. Haydon, *Proc. R. Soc. London, Ser. A*, 1975, **347**, 161–177.
37 D. E. Brooks, Y. K. Levine, J. Requena and D. A. Haydon, *Proc. R. Soc. London, Ser. A*, 1975, **347**, 179–194.
38 S. H. White, *Biophys. J.*, 1975, **15**, 95–117.
39 E. Bamberg and R. Benz, *Biochim. Biophys. Acta, Biomembr.*, 1976, **426**, 570–580.
40 R. Benz and K. Janko, *Biochim. Biophys. Acta, Biomembr.*, 1976, **455**, 721–738.
41 O. Alvarez and R. Latorre, *Biophys. J.*, 1978, **21**, 1–17.
42 S. White, *Biophys. J.*, 1978, **23**, 337–347.
43 D. Bach and I. Miller, *Biophys. J.*, 1980, **29**, 183.
44 T. J. McIntosh, S. A. Simon and R. C. MacDonald, *Biochim. Biophys. Acta, Biomembr.*, 1980, **597**, 445–463.
45 J. P. Dilger, *Biochim. Biophys. Acta, Biomembr.*, 1981, **645**, 357–363.
46 H. Bayley, B. Cronin, A. Heron, M. A. Holden, W. L. Hwang, R. Syeda, J. Thompson and M. Wallace, *Mol. BioSyst.*, 2008, **4**, 1191–1208.
47 G. Villar, A. J. Heron and H. Bayley, *Nat. Nanotechnol.*, 2011, **6**, 803–808.
48 G. Villar, A. D. Graham and H. Bayley, *Science*, 2013, **340**, 48–52.
49 N. Malmstadt, M. A. Nash, R. F. Purnell and J. J. Schmidt, *Nano Lett.*, 2006, **6**, 1961–1965.
50 J. Poulos, S. Portonovo, H. Bang and J. Schmidt, *J. Phys.: Condens. Matter*, 2010, **22**, 454105.
51 J. L. Poulos, T.-J. Jeon, R. Damoiseaux, E. J. Gillespie, K. A. Bradley and J. J. Schmidt, *Biosens. Bioelectron.*, 2009, **24**, 1806–1810.
52 J. L. Poulos, W. C. Nelson, T.-J. Jeon, C.-J. Kim and J. J. Schmidt, *Appl. Phys. Lett.*, 2009, **95**, 013706.
53 T. Thapliyal, J. L. Poulos and J. J. Schmidt, *Biosens. Bioelectron.*, 2011, **26**, 2651–2654.
54 S. A. Sarles and D. J. Leo, *Anal. Chem.*, 2010, **82**, 959–966.
55 L. C. M. Gross, O. K. Castell and M. I. Wallace, *Nano Lett.*, 2011, **11**, 3324–3328.
56 G. J. Taylor and S. A. Sarles, *Langmuir*, 2015, **31**, 325–337.
57 W. L. Hwang, M. Chen, B. d. Cronin, M. A. Holden and H. Bayley, *J. Am. Chem. Soc.*, 2008, **130**, 5878–5879.
58 M. A. Holden, D. Needham and H. Bayley, *J. Am. Chem. Soc.*, 2007, **129**, 8650–8655.
59 W. L. Hwang, M. A. Holden, S. White and H. Bayley, *J. Am. Chem. Soc.*, 2007, **129**, 11854–11864.

60 Y. Elani, R. V. Law and O. Ces, *Nat. Commun.*, 2014, **5**, 5305.
61 Y. Elani, R. V. Law and O. Ces, *Phys. Chem. Chem. Phys.*, 2015, **17**, 15534–15537.
62 A. J. Heron, J. R. Thompson, A. E. Mason and M. I. Wallace, *J. Am. Chem. Soc.*, 2007, **129**, 16042–16047.
63 A. Fischer, M. A. Holden, B. L. Pentelute and R. J. Collier, *Proc. Natl. Acad. Sci. U. S. A.*, 2011, **108**, 16577–16581.
64 J. B. Boreyko, G. Polizos, P. G. Datskos, S. A. Sarles and C. P. Collier, *Proc. Natl. Acad. Sci. U. S. A.*, 2014, **111**, 7588–7593.
65 N. Stuurman, A. D. Edelstein, N. Amodaj, K. H. Hoover and R. D. Vale, in *Current protocols in molecular biology*, ed. F. M. Ausubel, *et al.*, 2010, Unit14. 20.
66 A. R. Thiam, N. Bremond and J. Bibette, *Phys. Rev. Lett.*, 2011, **107**, 068301.
67 A. D. Petelska and Z. A. Figaszewski, *Bioelectrochem. Bioenerg.*, 1998, **46**, 199–204.
68 R. Shamai, D. Andelman, B. Berge and R. Hayes, *Soft Matter*, 2008, **4**, 38–45.
69 S. Chevalliot, S. Kuiper and J. Heikenfeld, *J. Adhes. Sci. Technol.*, 2012, **26**, 1909–1930.
70 F. Mugele and J.-C. Baret, *J. Phys.: Condens. Matter*, 2005, **17**, R705.
71 A. Quinn, R. Sedev and J. Ralston, *J. Phys. Chem. B*, 2005, **109**, 6268–6275.
72 J. C. Weaver and Y. A. Chizmadzhev, *Bioelectrochem. Bioenerg.*, 1996, **41**, 135–160.
73 S. White and W. Chang, *Biophys. J.*, 1981, **36**, 449.
74 J. Requena, D. A. Haydon and S. B. Hladky, *Biophys. J.*, 1975, **15**, 77–81.
75 S. Punnamaraju, H. You and A. J. Steckl, *Langmuir*, 2012, **28**, 7657–7664.
76 G. Valincius, F. Heinrich, R. Budvytyte, D. J. Vanderah, D. J. McGillivray, Y. Sokolov, J. E. Hall and M. Lösche, *Biophys. J.*, 2008, **95**, 4845–4861.
77 P. Poulin and J. Bibette, *Langmuir*, 1998, **14**, 6341–6343.
78 E. Baykal-Caglar, E. Hassan-Zadeh, B. Saremi and J. Huang, *Biochim. Biophys. Acta, Biomembr.*, 2012, **1818**, 2598–2604.
79 C. Karolis, H. G. L. Coster, T. C. Chilcott and K. D. Barrow, *Biochim. Biophys. Acta, Biomembr.*, 1998, **1368**, 247–255.
80 T. P. W. McMullen, R. N. A. H. Lewis and R. N. McElhaney, *Biochemistry*, 1993, **32**, 516–522.
81 S. Chiu, E. Jakobsson, R. J. Mashl and H. L. Scott, *Biophys. J.*, 2002, **83**, 1842–1853.
82 Y. Suzuki, *J. Lipid Res.*, 1982, **23**, 62–69.
83 I. W. Levin, E. Keihn and W. C. Harris, *Biochim. Biophys. Acta, Biomembr.*, 1985, **820**, 40–47.

